ENHANCED VISUALIZATION OF HYPERSPECTRAL IMAGES

Z. Mahmood, P. Scheunders

IBBT-Vision Lab
Department of Physics
University of Antwerp, Belgium

1. INTRODUCTION

Hyperspectral (HS) images employ hundreds of contiguous spectral bands to capture and process spectral information over a range of wavelengths, allowing for a better classification and discrimination. To display a hyperspectral image on standard color display, its dimensionality needs to be reduced to three (Red, Green and Blue (RGB)) channels. This enables humans to quickly browse through the image, e.g. to find regions of interest and relevant features in the image for further analysis by the computer.

In the literature, a number of statistical methods to convert the hyperspectral images to RGB composite images were described. Principal Component Analysis (PCA) [1] is the most widely used method to map an arbitrary number of bands into an RGB image. The eigenvectors corresponding to the principal component images sample the entire spectral range. It is common to map the first three principal components into an RGB image. In [2] and [3] partitioned principal component analysis methods were proposed to reduce the number of bands to display the hyperspectral images. Another method proposed to use a combination of PCA and optimization [4]. PCA-based methods work well if the signals can be modeled in terms of their 2-nd order statistics. But hyperspectral images require higher order statistics and dimensionality reduction methods based on independent component analysis have been proposed for visualization purposes [5], [6]. One drawback of PCA is that it does not incorporate the spatial relations among image pixels. In [7] modifications of PCA are suggested to exploit the spatial relations among pixels. In [8] a tensor based method is proposed to jointly take advantage of spatial and spectral information for dimensionality reduction. In [9], [10] and [11] a human vision system (HVS) model is used. Hyperspectral images are linearly projected onto basis functions designed for RGB primaries of a standard tristimulus display. These latter techniques lead to results most resembling images acquired with a standard RGB color camera.

In this work, we propose a hyperspectral image visualization technique, integrating a contrast enhancement procedure into the HVS projection technique. In this way, an enhanced color image is obtained with improved contrast for an improved visual inspection.

2. ENHANCED HYPERSPECTRAL IMAGE VISUALIZATION

In Fig. 1, the proposed technique is schematically shown. The proposed visualization algorithm is based on a vector-valued image wavelet representation known as multiscale fundamental form (MFF) [12]. First, all image bands are wavelet transformed. MFF describes the multiscale gradient of a vector-image. Applied on a hyperspectral image, MFF compresses detail subbands of all the image bands into one subband that describes the multiscale gradient of the image at that particular scale and subband. Since the noise of each band is accumulated as well in the MFF, a denoising step is applied. The low resolution bands are linearly projected onto HVS color matching functions [10] to get the three low resolution images L_R, L_G and L_B. Finally the inverse wavelet transform is applied to obtain the RGB composite image suitable for display.

2.1. Multiscale Fundamental Form

A detailed description of MFF is given in [12]. Let $\mathbf{I}(x, y)$ be a hyperspectral image with components $I_i(x, y), i = 1, \ldots, N$. The wavelet transform employed is based on non-orthogonal (redundant) discrete wavelet frames introduced by Mallat [13]. The wavelet transform of band i is defined by:

$$D^x_{i,s}(x, y) = I_i * \psi^x_s(x, y) \text{ and } D^y_{i,s}(x, y) = I_i * \psi^y_s(x, y) \tag{1}$$

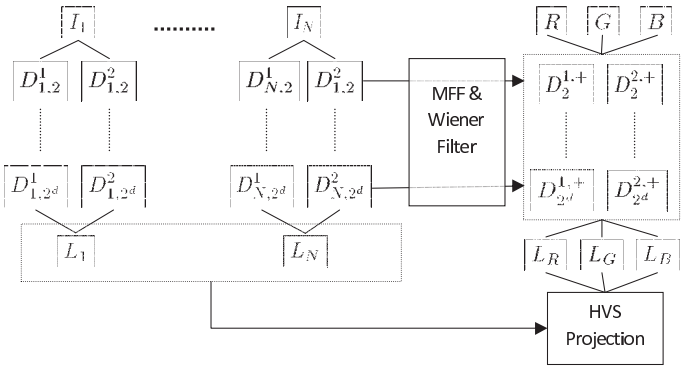

Fig. 1. Enhanced Hyperspectral Image Visualization Algorithm

where $*$ denotes the convolution operator and the functions $\psi_s^{x,y}(x,y)$ are scaled and delated functions of the mother wavelets, which are derivatives with respect to x and y of a smoothing function. s is the scale parameter which commonly is set equal to 2^j with $j = 1, \ldots, d$.

The square norm of the differential of $\mathbf{I}(x,y)$ is given by the following expression:

$$[d(\mathbf{I} * \theta_{2^j})]^2 = 2^{-2j} \begin{pmatrix} dx \\ dy \end{pmatrix}^T \begin{bmatrix} \sum (D^1_{n,2^j})^2 & \sum D^1_{n,2^j} D^2_{n,2^j} \\ \sum D^1_{n,2^j} D^2_{n,2^j} & \sum (D^2_{n,2^j})^2 \end{bmatrix} \begin{pmatrix} dx \\ dy \end{pmatrix} \tag{2}$$

where $D^1_{n,2^j}$ and $D^2_{n,2^j}$ are the jth-scale detail coefficients of the nth band image. The matrix in this expression is the MFF and represents the gradient information at the jth scale.

2.2. Noise Estimation And Wiener Filtering

A problem with the MFF is that the noise in each detail subband is accumulated. When the noise in each band is assumed to be Gaussian independent with a standard deviation of σ, then the noise of each wavelet subband is given by $\sigma_j = \|\psi_j\|\sigma$. It can be shown that for large values of N the diagonal terms in the MFF approximate the gaussian function $g(N\sigma_j^2, 2N\sigma_j^4)$ and the off-diagonal terms approximate the gaussian function $g(\frac{N}{2}\sigma_j^2, N\sigma_j^4)$ [14]. To remove the noise, a Wiener filter based on these Gaussian models is applied to the matrix elements.

2.3. HVS projection

The hyperspectral image can be represented at each scale by

$$\begin{aligned} D^{1,+}_{2^j}(x,y) &= \sqrt{\lambda^+_{2^j}}\, \upsilon^+_{2^j,x}(x,y), \\ D^{2,+}_{2^j}(x,y) &= \sqrt{\lambda^+_{2^j}}\, \upsilon^+_{2^j,y}(x,y). \end{aligned} \tag{3}$$

with $\lambda^+_{2^j}$ and $\upsilon^+_{2^j,x}(x,y)$ the largest eigenvalue and corresponding eigenvector of the multiscale fundamental form [12]. Let r, g and b be discrete basis functions, corresponding to the HVS color matching functions [10]. $L_i, i = 1, \ldots, N$ are low resolution images of the original bands. The low resolution images corresponding to red (R), green (G) and blue (B) components are obtained by linear projection of L_i onto each basis functions.

$$L_R = r^T L_i \;\; L_G = g^T L_i \;\; L_B = b^T L_i \tag{4}$$

By applying the inverse wavelet transform, the R,G and B components of the composite RGB image are obtained.

3. RESULTS AND CONCLUSION

We performed several experiments to validate our visualization algorithm, using hyperspectral images of natural scenes [15].These hyperspectral images were acquired with a progressive-scanning monochrome digital camera with a tunable birefringent filter mounted in front of the lens. The wavelength range of 410-710 nm was sampled at 10-nm intervals so that an

image consisted of 31 bands. Experiments were also performed with 224-band AVIRIS hyperspectral images. We compared our algorithm with the HVS projection only algorithm [10]. Fig. 2(a) and (b) show the results of applying HVS projection and our algorithm respectively to an image of a natural scene. Similarly Fig. 3(a) and (b) show the results of applying HVS projection and our algorithm respectively to a 224-band AVIRIS image. Some noisy bands and bands having no data were discarded. For both images, one can clearly observe a general sharper image with improved contrast when using our technique compared to the HVS-projection technique. Also for both images hue remains the same as in HVS-projection technique, indicating that design goals defined in [10] are still satisfied. The presented technique is scalable with respect to the number of bands that is applied in the MFF. The more bands applied the higher the contrast improvement will be. Also the choice of the applied bands is free, allowing to select specific spectral regions for enhancement. Finally, the number of scales applied in the wavelet transform also determines the degree of contrast improvement.

(a) HVS Projection (b) MFF Visualization

Fig. 2. Visualization of Hyperspectral Image of a Natural Scene.

(a) HVS Projection (b) MFF Visualization

Fig. 3. Visualization of Hyperspectral AVIRIS Image.

4. REFERENCES

[1] J. S. Tyo, A. Konsolakis, D. I. Diersen, and R. C. Olsen, "Principal-components-based display strategy for spectral imagery," vol. 41, no. 3, pp. 708–718, Mar. 2003.

[2] V. Tsagaris, V. Anastassopoulos, and G. A. Lampropoulos, "Fusion of hyperspectral data using segmented pct for color representation and classification," vol. 43, no. 10, pp. 2365–2375, Oct. 2005.

[3] Xiuping Jia and J. A. Richards, "Segmented principal components transformation for efficient hyperspectral remote-sensing image display and classification," vol. 37, no. 1, pp. 538–542, Jan. 1999.

[4] Ming Cui, A. Razdan, Jiuxiang Hu, and P. Wonka, "Interactive hyperspectral image visualization using convex optimization," vol. 47, no. 6, pp. 1673–1684, June 2009.

[5] Jing Wang and Chein-I Chang, "Independent component analysis-based dimensionality reduction with applications in hyperspectral image analysis," vol. 44, no. 6, pp. 1586–1600, June 2006.

[6] Yingxuan Zhu, P. K. Varshney, and Hao Chen, "Evaluation of ica based fusion of hyperspectral images for color display," in *Proc. 10th International Conference on Information Fusion*, July 9–12, 2007, pp. 1–7.

[7] M. R. Gupta and N. P. Jacobson, "Wavelet principal component analysis and its application to hyperspectral images," in *Proc. IEEE International Conference on Image Processing*, Oct. 8–11, 2006, pp. 1585–1588.

[8] N. Renard and S. Bourennane, "Dimensionality reduction based on tensor modeling for classification methods," vol. 47, no. 4, pp. 1123–1131, Apr. 2009.

[9] N. P. Jacobson, M. R. Gupta, and J. B. Cole, "Linear fusion of image sets for display," vol. 45, no. 10, pp. 3277–3288, Oct. 2007.

[10] N. P. Jacobson and M. R. Gupta, "Design goals and solutions for display of hyperspectral images," vol. 43, no. 11, pp. 2684–2692, Nov. 2005.

[11] N. P. Jacobson and M. R. Gupta, "Snr-adaptive linear fusion of hyperspectral images for color display," in *Proc. IEEE International Conference on Image Processing ICIP 2007*, Sept. 2007, vol. 3, pp. III–477–III–480.

[12] P. Scheunders, "A multivalued image wavelet representation based on multiscale fundamental forms," vol. 11, no. 5, pp. 568–575, May 2002.

[13] S. Mallat and S. Zhong, "Characterization of signals from multiscale edges," vol. 14, no. 7, pp. 710–732, July 1992.

[14] P. Scheunders, "Wavelet thresholding of multivalued images," vol. 13, no. 4, pp. 475–483, Apr. 2004.

[15] Ferreira F. Nascimento, S.M.C. and D.H. Foster, "Statistics of spatial cone-excitation ratios in natural scenes," *Journal of the Optical Society of America A*, vol. 19, pp. 1484–1490, 2002.